Molecular Crystals and Liquid Crystals

Publication details, including instructions for authors and subscription information:
http://www.tandfonline.com/loi/gmcl20

Reentrant EHC Patterns Under Superimposed Square Wave Excitation

Jana Heuer [a], Ralf Stannarius [a] & Thomas John [b]

[a] Otto-von-Guericke-Universität Magdeburg, Institut für Experimentelle Physik

[b] Carl-von-Ossietzky-Universität Oldenburg, Institut für Physik

Version of record first published: 31 Aug 2006

To cite this article: Jana Heuer, Ralf Stannarius & Thomas John (2006): Reentrant EHC Patterns Under Superimposed Square Wave Excitation, Molecular Crystals and Liquid Crystals, 449:1, 11-19

To link to this article: http://dx.doi.org/10.1080/15421400600579875

Mol. Cryst. Liq. Cryst., Vol. 449, pp. 11–19, 2006

ISSN: 1542-1406 print/1563-5287 online
DOI: 10.1080/15421400600579875

Taylor & Francis
Taylor & Francis Group

Reentrant EHC Patterns Under Superimposed Square Wave Excitation

Jana Heuer
Ralf Stannarius
Otto-von-Guericke-Universität Magdeburg, Institut für Experimentelle Physik

Thomas John
Carl-von-Ossietzky-Universität Oldenburg, Institut für Physik

The presented study deals with pattern forming phenomena in electrohydrodynamic convection (EHC) under superimposed rectangular wave forms. An effect of re-stabilization is observed experimentally, i.e., with changing of one control parameter of the excitation wave form, the system undergoes transitions from the convecting state through the non-convecting ground state back into the convecting state. We provide a theoretical explanation for this behavior using a model based on two coupled homogenous differential equations.

Keywords: electroconvection; spontaneous pattern formation; stability analysis

1. INTRODUCTION

Electrohydrodynamic convection (EHC) in nematic liquid crystals is a well known dissipative pattern forming system. Particularly, the classical so-called conduction and dielectric pattern regimes have been subject of numerous studies and monographs, e.g., [1–3]. Recently a subharmonic regime has been characterized in [4,5].

Based on the ground state, the nematic director $\bar{n}$ is preferably oriented along the x axis (Fig. 1). Applying a subcritical electric field E normal to the cell, the ground state remains stable. When a certain critical field E_c is reached, convective flow sets in and the director $\bar{n}$ will be periodically deflected to form an angle φ with respect to the cell

Address correspondence to Jana Heuer, Otto-von-Guericke-Universität Magdeburg, Institut für Experimentelle Physik, Universitätsplatz 2, 39106 Magdeburg, Germany. E-mail: jana.heuer@gast.uni-magdeburg.de

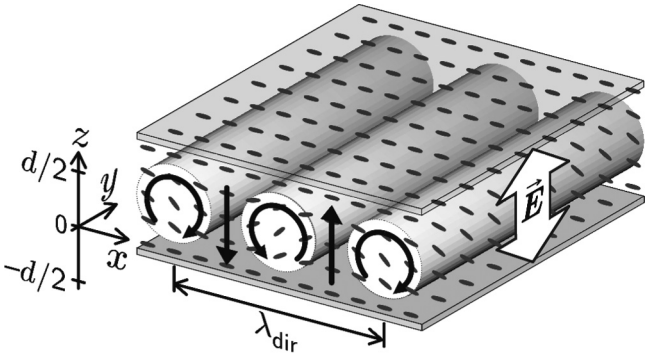

FIGURE 1 Schematic picture of the electroconvection rolls in the conduction regime with a spatial wave length λ_{dir}. The electric field $\vec{E}(t)$ is applied normal to the cell. Circular arrows sketch the convective flow, up and down arrows indicate the ionic charge transport. The cell gap d used in our experiments is 48.5 μm.

plane. Responsible for that is the coupling between the liquid crystal convective flow and the flow of ions contained due to impurities.

Fundamental for the selection of the different pattern regimes is the excitation wave form: shape, frequency and voltage. Classical EHC studies consider typically sinus and square waves or stochastic excitations. One can establish a threshold diagram that contains two parameters of a fixed excitation wave form, e.g., frequency and voltage in the case of a simple wave form like square or sinus. In the case of superposition of simple wave forms one can choose, for example, the amplitudes of two superimposed square waves with fixed frequencies and phase shift as parameters. To get such a diagram, experimentally as well as theoretically, for every data point one of these parameters is kept fixed, while the other is varied and the onset is marked.

Superposition of wave forms has been studied by several authors, one interesting aspect, e.g., is the superposition of a deterministic excitation with noise. Depending on the frequency, the superimposed excitation wave can stabilize or destabilize the ground state. Müller and Behn, for example, have studied the superposition of a constant field with a stochastic square wave field of a certain finite correlation time theoretically [6]. It has been found in these studies that a superimposed driving field may first stabilize the non-convecting ground state, and at higher amplitudes destabilize this ground state again. With the stability criterion chosen by these authors, it was predicted that the re-stabilization characteristics depends crucially on the mean number

of jumps α of the stochastic voltage and on the dimensionless Helfrich parameter ζ^2 that includes dielectric constants, conductivities and viscosities of the material.

There has not been an experimental confirmation of these theoretical investigation so far. In our experiment, we consider the superposition of two deterministic fields, i.e., two rectangular waves where the slow component is always chosen below the cut-off, the fast one above the cut-off. In order to avoid beating, a ratio of 1:4 of both frequencies has been chosen. The phase shift has been selected so that the upward slopes of the slow frequency coincide with upward slopes of the fast frequency. For other frequency ratios, in particular odd integer ratios, and for other phase shifts, the pattern state diagram can be qualitatively different.

2. MODEL

2.1. Basic Equations

The EHC-System can be modeled by two coupled homogenous differential equations, where the space charge density q and the director deflection φ are the essential dynamic variables. Constitutive for this model, described e.g., in [1,2,7,8], is the balance of the elastic, dielectric and viscous torques on the director.

Furthermore, a test mode ansatz is chosen that describes normal rolls (wave vector along the preferred director ground state):

$$\begin{aligned} \widetilde{\varphi}(x,z,t) &= \varphi(t)\cos(k_x x)\cos(k_z z), \\ \widetilde{q}(x,z,t) &= q(t)\sin(k_x x)\cos(k_z z) \end{aligned} \tag{1}$$

where $k_x = 2\pi/\lambda_{dir}$ is the wave number of the spatial test mode of the pattern in the cell plane and $k_z = \pi/d$ the wave number with respect to the cell normal with consideration of strong anchoring at the glass slides. This leads to a set of two linearized equations

$$\frac{\mathrm{d}}{\mathrm{d}t}\begin{pmatrix} q(t) \\ \varphi(t) \end{pmatrix} + \begin{pmatrix} a_1 & a_2 E(t) \\ a_3 E(t) & a_4 + a_5 E^2(t) \end{pmatrix}\begin{pmatrix} q(t) \\ \varphi(t) \end{pmatrix} = 0. \tag{2}$$

The evolution matrix depends upon the applied electric field $E(t) = U(t)/d$ and its coefficients a_i depend on the material parameters of the nematic liquid crystal to be analyzed and on the test mode wave number k_x (details e.g., in [9]).

Under driving with piecewise constant periodic wave forms, these equations can be straightforwardly integrated and the evolution of the pattern amplitude can be determined analytically. The Floquet

theorem leads to solutions described in [4]. After solving this set of equations, the two eigen-values $\mu_{1,2}$, calculated over one period T of the excitation field, are conventionally written in the form $\mu_i = e^{\lambda_i T}$, $i = 1, 2$. We sort the exponents such that $\mathrm{Re}[\lambda_1] > \mathrm{Re}[\lambda_2]$, where λ_1 determines the asymptotic behavior of the respective test mode with wave number k_x. Consequently, it is sufficient to analyze the multiplier μ_1 for the stability analysis. The Floquet multiplier μ_1 is presented in the stability diagrams of the next subsection, where μ_1 depends both on the wave number and the excitation sequence, which is parameterized.

At simple square wave excitation, the electric field amplitude E (or voltage amplitude U) is used as the relevant parameter and the mode with lowest threshold E is expected to dominate the pattern periodicity at onset. In the case of superposition of two square waves, we fix one of these amplitudes and take the second one as the parameter in the $\mu_1(U, k_x)$ diagrams. There, regions with $|\mu_1| > 1$ correspond to unstable modes.

2.2. Theoretical Predictions

The diagrams of Figure 2 are calculated with the material parameters of the nematic Mischung 5 (data see [9]) for the superposition of two square wave fields with the frequencies $f_{\mathrm{high}} = 120\,\mathrm{Hz}$ and $f_{\mathrm{low}} = 30\,\mathrm{Hz}$. In each diagram, the amplitude U_{high} of the component with frequency f_{high} is fixed. It turns out that μ_1 is real everywhere except for some very small regions in the vicinity of the curve S (shown in Figure 2 as dash-dotted line). Since $|\mu_1| < 1$ there, this region is irrelevant for the stability analysis. Presented are regions with $0 < \mu_1 < 1$ (white) where the ground state is stable, and regions with $\mu_1 > 1$ (light gray) that correspond to conduction and dielectric patterns, where the system variables are periodic with the low frequency component of the excitation. Furthermore, there are regions with $\mu_1 < -1$ (dark gray) that correspond to the subharmonic regime where director deflection and charge density follow the double period of the low frequency component of the excitation. The region with $-1 < \mu_1 < 0$ that corresponds to subharmonic solutions with negative growth rates is surrounded by the separatrix S where $\mathrm{Re}[\mu_1] = 0$ [4,5]. The neutral curve N (solid line in 2) is defined by $|\mu_1| = 1$. The global minimum of N with the critical values of voltage $U_{\mathrm{low,c}}$ and wave number $k_{x,\mathrm{c}}$ specifies the pattern onset. The topology of the stability diagram changes continuously with the excitation parameters.

Diagram 2(a) shows a situation where the global minimum of N is found for conduction patterns. With increasing voltage U_{high} in

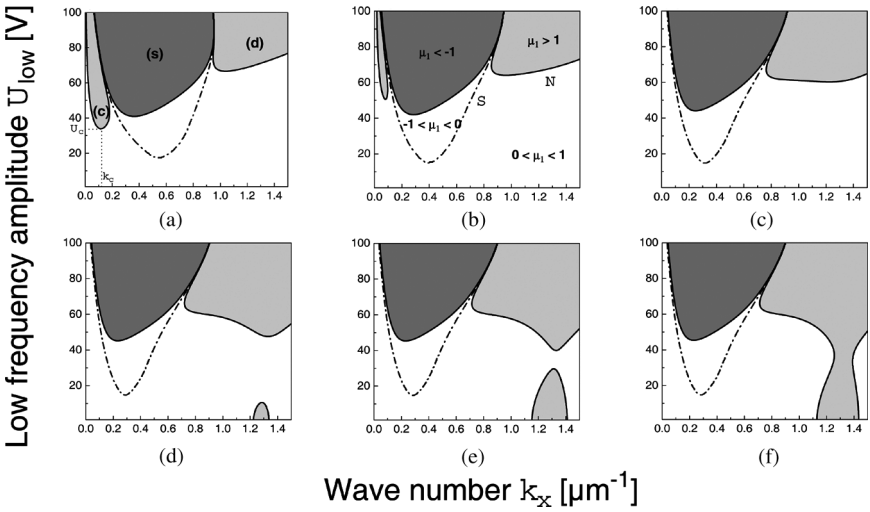

FIGURE 2 Calculated stability diagrams of the superposition of two square waves with frequencies $f_{\text{high}} = 120\,\text{Hz}$ and $f_{\text{low}} = 30\,\text{Hz}$. The diagrams (a)–(f) correspond to fixed voltages $U_{\text{high}} = 72\,\text{V}$, 86 V, 94 V, 97.2 V, 97.6 V, 97.8 V respectively. Presented are the regions with conduction (c), subharmonic (s) and dielectric (d) solutions and the respective ranges of μ_1 whereas $\mu_1 > 1$ in the light gray regions and $\mu_1 < -1$ in the dark gray regions. The separatrix S is presented by the dashed line, the neutral curve N, whose global minimum leads to the threshold voltage an the critical wave number, by the solid lines.

diagrams (b) and (c), the conduction pattern region disappears and the subharmonic region gives the global minimum of the neutral curve. Therefore, subharmonic convection rolls appear at onset. In diagrams (d) and (e), with further increasing of U_{high}, the region corresponding to the dielectric regime provides the lowest threshold. Here, the selected wave numbers $k_{x,\text{c}}$ belong to two extrema of the neutral curve N. Diagrams (d) and (e) lead to two threshold voltages $U_{\text{low,c}}$, with two nearly equal wave numbers $k_{x,\text{c}}$. Finally, in diagram (f) the ground state of the system is unstable with respect to dielectric patterns for any U_{low}.

The values of the global extremum of the neutral curve for each voltage U_{high} produce the threshold diagram in Figure 3. These results lead to a prediction of a re-entry phenomenon: Above a certain high frequency voltage U_{high} (97.1 V in Fig. 3), the ground state is unstable with respect to the formation of dielectric patterns already at $U_{\text{low}} = 0$. With increasing U_{low}, the ground state becomes stable. For still higher values of U_{low} the system re-enters the dielectric pattern regime.

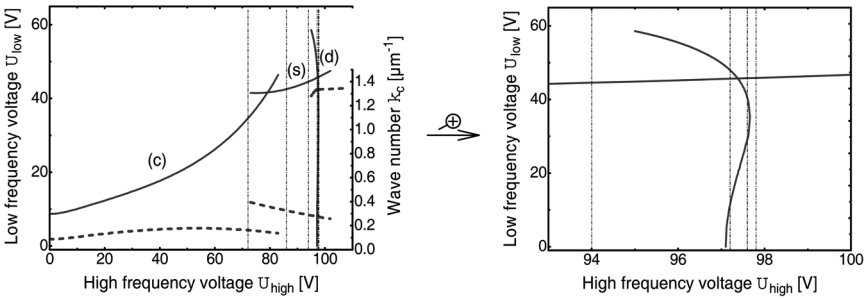

FIGURE 3 Calculated threshold diagram with critical wave numbers of the superposition of two square waves with $f_{\text{high}} = 120\,\text{Hz}$ and $f_{\text{low}} = 30\,\text{Hz}$. (c), (s) and (d) represent the different pattern regimes conduction, subharmonic and dielectric. The right diagram is the extended range of the interesting values of U_{high}. The dash-dotted lines mark the parameters where the diagrams of Figure 2 have been calculated.

In Figure 4 the calculated threshold diagrams for several frequency pairs of the superimposed square waves are presented. All frequency combinations have the same ratio of 1:4. One can realize the vanishing

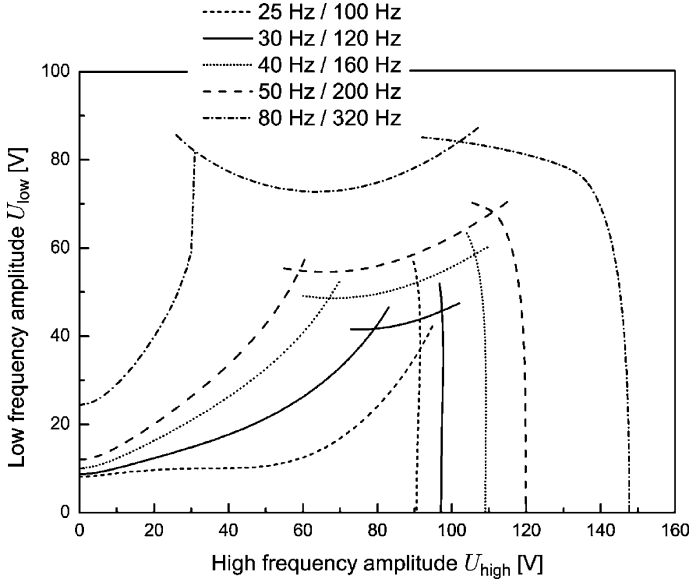

FIGURE 4 Calculated threshold curves for different superimposed square wave excitations with a frequency ratio of 1:4. In the legend, the frequency pairs $f_{\text{low}}/f_{\text{high}}$ are labeled.

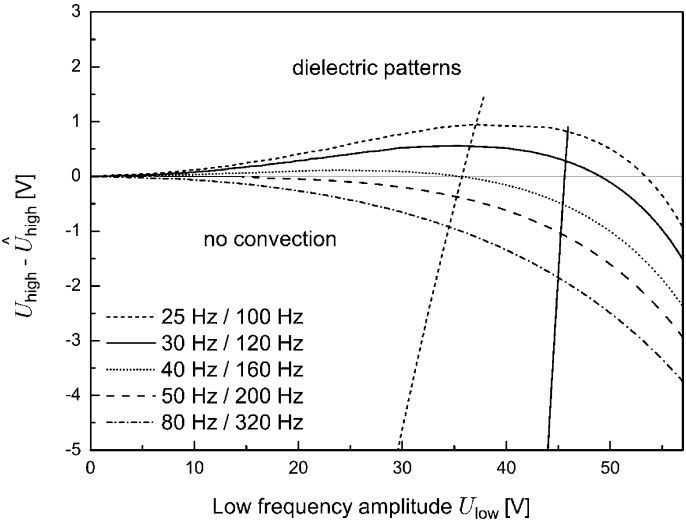

FIGURE 5 Interesting range of U_{high} of Figure 4 versus the threshold voltage U_{low}. The values of U_{high} are normalized to the threshold value $\widehat{U}_{\text{high}}$ for pattern onset at $U_{\text{low}} = 0$. In the legend, the frequency pairs $f_{\text{low}}/f_{\text{high}}$ are labeled.

of the subharmonic region with lower frequencies and the disappearing re-entry phenomenon for higher frequency pairs.

Figure 5 emphasizes this last aspect. Presented is the dielectric branch of Figure 4 at higher values of U_{high} where these values are normalized to the respective threshold value of U_{high} at $U_{\text{low}} = 0$. The curve belonging to low frequencies shows a definitive re-entrant behavior while this property disappears gradually with higher frequencies. Increasing of both frequencies supports the generation of dielectric patterns, the re-stabilization of the ground state is retarded more and more. On the other hand, the decrease of both frequencies supports the generation of conduction patterns, so that the subharmonic range becomes smaller and vanishes.

3. EXPERIMENTAL RESULTS

Experiments have been performed with the shadowgraph method using the material Mischung 5, all parameters and experimental conditions are described in references [5,9,10,11]. The experimental observation of the EHC patterns excited by two superposed square wave fields with the frequencies $f_{\text{high}} = 120\,\text{Hz}$ and $f_{\text{low}} = 30\,\text{Hz}$ leads to the threshold diagram in Figure 6. This diagram is measured at a

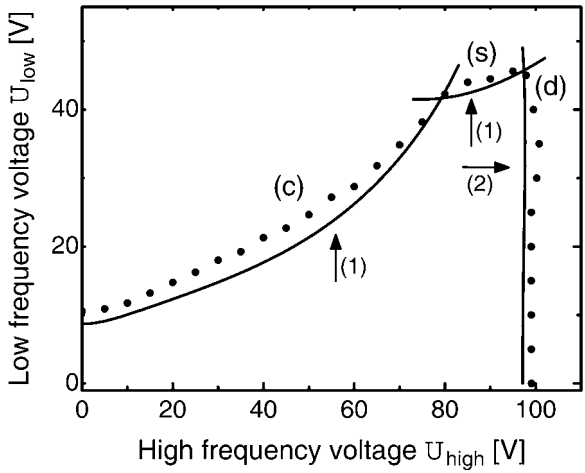

FIGURE 6 Experimental threshold diagram for $f_{high} = 120\,Hz$ and $f_{low} = 30\,Hz$. Presented are measured (•) and calculated values (–). (c), (s), (d) mark the different regimes: conduction, subharmonic and dielectric, respectively. The arrows indicate the experimental path in the parameter space: increasing U_{low} at fixed U_{high} (1) and increasing U_{high} at fixed U_{low} (2). The error bars are smaller than the size of the symbols.

fixed high frequency amplitude U_{high} while U_{low} is increased until convection sets in (arrow 1). In order to determine the threshold voltages in the bump of the right hand sight of Figure 6, U_{low} was fixed and U_{high} was varied (arrow 2).

The experimental results confirm the existence of the re-entry phenomenon predicted in section 2.2. Noticeable is the fact that the range where two threshold voltages exist is much larger in the experiment than in the theory, because the width of this region is $\Delta U_{high} = 1.8\,V$ experimentally and $\Delta U_{high} = 0.56\,V$ theoretically.

4. CONCLUSIONS

We have studied the superposition of square wave excitations by analysis of a system of model equations for EHC. The pattern state diagram is much more complex than for simple rectangular or sinusoidal driving fields, in particular it contains a subharmonic regime. At variation of one of the driving parameters, a re-stabilization of the ground state and subsequent re-entry into the convective state has been predicted. The effect is confirmed in experiments. Thereby we found a qualitatively agreement between experiment and theory

but we get a quantitative discrepancy. Since the theory is only a linearized model with crude assumptions on the test modes, it is not surprising that quantitative details are not exactly reproduced. The model describes the thresholds of the regimes (c), (s), (d) satisfactorily but is only qualitatively expedient when studying more complex effects.

REFERENCES

[1] Chandrasekhar, S. (1992). *Liquid Crystals*, second edition. Cambridge University Press.
[2] de Gennes, P. G. & Prost, J. (1993). *The physics of liquid crystals*, second edition. Clarendon Press: Oxford.
[3] Kramer, L. & Pesch, W. (1996). Electrohydrodynamic instabilities in nematic liquid crystals. In: *Pattern Formation in Liquid Crystals*, Buka A. & Kramer, L. (Eds.), Springer: New York, 221–225.
[4] John, T. & Stannarius, R. (2004). Preparation of subharmonic patterns in nematic electroconvection. *Phys. Rev., E 70*, 025202.
[5] John, T., Heuer, J., & Stannarius, R. Influence of excitation wave forms and frequencies on the fundamental time symmetry of the system dynamics, studied in nematic electroconvection, submitted to *Phys. Rev. E. 71*, 056307.
[6] Müller, R. & Behn, U. (1987). Electrohydrodynamic instabilities in nematic liquid crystals under dichotomous parametric modulation. *Z. Phys., B 69*, 185. This work uses a one-dimensional model, mode selection is not taken into account.
[7] Dubois-Violette, E., de Gennes, P. G., & Parodi, O. (1971). Hydrodynamic instabilities in nematic liquid crystals under a.c. electric fields. *J. de Physique*, *32*, 305.
[8] Bodenschatz, E., Zimmermann, W., & Kramer, L. (1988). On electrically driven pattern-forming instabilites in planar nematics. *J. Phys. France*, *49*, 1875.
[9] John, T., Behn, U., & Stannarius, R. (2003). Laser diffraction by periodic dynamic patterns in anisotropic fluids. *Eur. Phys. J., B 35*, 267.
[10] Rasenat, S., Hartung, G., Winkler, B. L., & Rehberg, I. (1989). The shadowgraph method in convection experiments. *Exp. Fluids*, *7*, 412.
[11] Plaut, E., Joets, A., & Ribotta, R. (1997). Optical characterization of the director field in a distorted nematic layer. *J. Phys. France*, *7*, 2459.